Synthesize multi-walled carbon nanotubes via catalytic chemical vapour deposition method on Fe-Ni bimetallic catalyst supported on kaolin

Article *in* Carbon letters · January 2017

DOI: 10.5714/CL.2017.21.033

CITATIONS
9

READS
802

6 authors, including:

AHMED ALIYU
Federal University Wukari
23 PUBLICATIONS **49** CITATIONS
SEE PROFILE

A. S. Abdulkareem
Federal University of Technology Minna
129 PUBLICATIONS **568** CITATIONS
SEE PROFILE

Abdulsalami Kovo
Federal University of Technology Minna
53 PUBLICATIONS **372** CITATIONS
SEE PROFILE

Jimoh Tijani Oladejo
Federal University of Technology Minna
44 PUBLICATIONS **397** CITATIONS
SEE PROFILE

CARBON letters

Original Articles
Carbon Letters Vol. 21, 33-50 (2017)

Synthesize multi-walled carbon nanotubes via catalytic chemical vapour deposition method on Fe-Ni bimetallic catalyst supported on kaolin

Aliyu A[1,2], Abdulkareem AS[1,2], Kovo AS[1], Abubakre OK[1,2], Tijani JO[2,3♠] and Kariim I[4]

[1]Department of Chemical Engineering, Federal University of Technology Minna, PMB 65, Niger State, Nigeria
[2]Nanotechnology Research Group, Center for Genetic Engineering and Biotechnology, Federal University of Technology Minna, PMB 65, Niger State, Nigeria
[3]Department of Chemistry, Federal University of Technology Minna, PMB 65, Niger State, Nigeria

Article Info
Received 23 August 2016
Accepted 6 October 2016

♠Corresponding Author
E-mail: jimohtijani@futminna.edu.ng
Tel: +23-480-5734-4464

DOI: http://dx.doi.org/10.5714/CL.2017.21.033

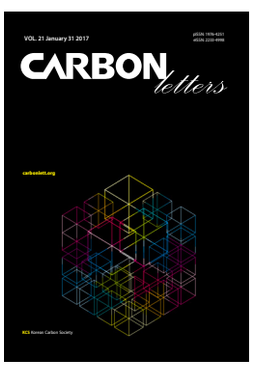

http://carbonlett.org

pISSN: 1976-4251
eISSN: 2233-4998

Abstract

In this study, Fe-Ni bimetallic catalyst supported on kaolin is prepared by a wet impregnation method. The effects of mass of kaolin support, pre-calcination time, pre-calcination temperature and stirring speed on catalyst yields are examined. Then, the optimal supported Fe-Ni catalyst is utilised to produce multi-walled carbon nanotubes (MWCNTs) using catalytic chemical vapour deposition (CCVD) method. The catalysts and MWCNTs prepared using the optimal conditions are characterized using high resolution transmission electron microscope (HRTEM), high-resolution scanning electron microscope (HRSEM), electron diffraction spectrometer (EDS), selected area electron diffraction (SAED), thermogravimetric analysis (TGA), Brunauer-Emmett-Teller (BET), and X-ray diffraction (XRD). The XRD/EDS patterns of the prepared catalyst confirm the formation of a purely crystalline ternary oxide ($NiFe_2O_4$). The statistical analysis of the variance demonstrates that the combined effects of the reaction temperature and acetylene flow rate predominantly influenced the MWCNT yield. The N_2 adsorption (BET) and TGA analyses reveal high surface areas and thermally stable MWCNTs. The HRTEM/HRSEM micrographs confirm the formation of tangled MWCNTs with a particle size of less than 62 nm. The XRD patterns of the MWCNTs reveal the formation of a typical graphitized carbon. This study establishes the production of MWCNTs from a bi-metallic catalyst supported on kaolin.

Key words: Multi-walled carbon nanotubes, kaolin, wet impregnation, factorial design, catalyst, catalytic chemical vapour deposition.

1. Introduction

Since early 1991, the design, synthesis, and characterization of nanostructured materials, particularly carbon nanotubes (CNTs), has received considerable attention among researchers due to their potential applications as nanoelectronic devices, in gas sensors, controlled drug release, water purification, hydrogen storage, reinforced composites, electrodes for fuel cells, and numerous other applications [1]. CNTs are extraordinary nanostructured materials with distinct tubular structures and large length/diameter ratios that are well-known for their remarkable electrical and thermal properties, and mechanical strength in the field of material science [2].

To date, several methods have been successfully tested and reported for the production of CNTs, which include arc discharge [3], laser ablation, electrolysis, and chemical vapor deposition (CVD; plasma-enhanced, thermal, and catalytic) [4,5]. Considerable research has been conducted using the first two techniques to produce high quality CNTs; nevertheless, the significant drawbacks of these techniques include high operat-

ing temperatures, high equipment costs, and difficulty in scaling-up for commercial purposes. In contrast, the production of CNTs via catalytic chemical vapor deposition (CCVD) remains the most dominant, ideal, cost effective, versatile, and transferable method of producing high quality and large quantity CNTs at relatively low synthesis temperatures [2-6]. This technique provides a unique opportunity to tailor and adjust the multi-structural parameters such as the diameter, length, and alignment in order to obtain well-defined and organized arrays of CNTs with different morphologies [7]. In the CCVD process, different hydrocarbons (methane, ethylene, acetylene, benzene, toluene, and carbon monoxide) are flowed over a metal catalyst (Fe, Co, Ni, and Mo, as well as their alloys) or on supported substrates such as alumina, activated carbon, zeolite, silica, silicon carbide, sodium chloride, titania, clays, and magnesium oxide, among others [8].

These support materials offer a suitable location for CNT growth in a CVD reactor. However, the selection of a suitable catalyst and catalyst support is a prerequisite for successful CNT growth via the CVD method. The selection of a support is based on properties such as the inertness, high surface area, stability under reaction and regeneration conditions, and low synthesis cost. For example, Lee et al. [9] reported that high surface area porous and non-porous materials such as SiO_2, Al_2O_3, zeolites, $CaCO_3$, and TiO_2 provide excellent supports for catalytic CNT production.

Previous studies have revealed that, during synthesis, porous materials such as zeolite and silica accumulate a substantial amount of amorphous carbon, which affect the production of crystalline CNTs [3,8-10]. However, $CaCO_3$, which is a non-porous material, prevented the formation of amorphous carbon and hence stimulated selective CNT production. Thus, the catalyst support used in the substrate CVD process has an important function in influencing the catalyst activity. In addition, different transition metals possess diverse catalytic activities and different CNT qualities.

These transition metals, particularly Fe, Co, and Ni, and their alloys, have been reported to be suitable to obtain a high surface area and excellent catalytic activity in the CNTs with exceptional mechanical strength. Furthermore, the production of CNTs using the CCVD technique has been found to depend on the type of carbon source, catalyst, growth time, and growth temperature [6-8]. Previously, Shah and Tali [8] found that inert methane and carbon monoxide produced single-wall CNTs (SWCNTs), while Dia et al. [11] and Yardimci et al. [12] independently demonstrated that unsaturated hydrocarbons such as acetylene can be used for multi-walled CNT (MWCNT) growth. Similarly, Chiwaye et al. [13] and Liu et al. [14] concluded that acetylene gas remained the most reactive unsaturated hydrocarbon and was most frequently employed for the growth of MWCNTs.

Several support materials have been used on active metals to produce CNTs with different lengths and diameters, e.g., zeolites [15], silica (SiO_2) [16], alumina (Al_2O_3) [17], calcium carbonate ($CaCO_3$) [18], and magnesia (MgO) [19]. These active transition metals can exist alone (Fe, Co, Mo, and Ni) or as a bimetallic (Fe-Co, Ni-Fe, and Co-Ni), tri-metallic (Fe-Co-Ni, Co-Mo-Fe), or sometimes ternary (Fe-Co-Ni-Mo) catalyst [19]. However, the production of CNTs from a bimetallic catalyst supported on a substrate appears more promising due to the increase in the catalytic performance and enhanced CNT yield [16]. For example, Chiwaye et al. [13] and Mhlanga et al. [20] reported the use of $CaCO_3$ supported on a Fe-Co catalyst for effective MWCNT production using acetylene as the carbon source. The authors observed the presence of CaO in the synthesized MWCNTs due to the partial decomposition of $CaCO_3$. The stronger chemical interaction between Al_2O_3 and the metal catalyst was attributed to the oxidation process occurring at the catalyst–Al_2O_3 interface. Bahgat et al. [21] investigated the synthesis of MWCNTs obtained from a bimetallic catalyst (Fe-Co) supported on $CaCO_3$ and found that as the crystal sizes reduced at higher temperatures, the CNT yield increased with temperature increases. Similarly, Motchelaho et al. [22] produced MWCNTs from Fe-Co supported $CaCO_3$ using the CVD method and found that 10% Fe-loaded acid treated CNTs possessed better activity than unpurified CNTs.

In this study, low cost and locally available kaolin was used as a replacement catalyst support in the catalyst synthesis for the growth of MWCNTs. Kaolin is a low-shrink-swell, non-porous solid material, which is also known as kaolinite or china clay, and it is comprised of several mixed oxides such as Fe_2O_3, Al_2O_3, TiO_2, MgO, and SiO_2, among others. Kaolin was selected instead of the commercially available support substrates due to its ability to withstand high temperatures, its exceptional chemical resistance, and its impact of excellent mechanical strength in the catalyst and the CNTs. The choice of Fe-Ni as the catalyst was favored based on its high solubility and high rate of carbon diffusion at high temperatures. Furthermore, the literature review demonstrated that little or no information exists regarding MWCNT production via bimetallic catalyst supported on kaolin using a wet impregnation method. Furthermore, it is also evident that no study has investigated the complete optimization of factors that influence the yields of the catalyst and CNTs using 24 factorial designs. Moreover, the effect of the process parameters such as reaction temperature, reaction time, argon flow rate, and acetylene flow rate on the MWCNT production using CCVD methods and CNT yield using 24 factorial designs has not been fully explored. Therefore, the present study is focused on the preparation of Fe-Co catalysts supported on kaolin using the wet impregnation method and subsequently followed by the CCVD of acetylene on the supported catalyst.

2 Experimental

2.1. Materials

The kaolin used in this study was sourced from Kankara, Kastina State, Nigeria, and used without further treatment or modification. All chemicals were supplied by Sigma Aldrich: $Fe(NO_3)_3$. $9H_2O$, $Ni(NO_3)_2.6H_2O$, NaOH, and HNO_3 were of analytical grade with 99.99% purity. The carbon source (C_2H_2) and carrier gas (Ar) with 99.99% purity were supplied by BOC Gases Nigeria Plc and were of analytical grade

Table 1. Variation of parameters for the 2^4 factorial designs for the catalyst preparation

Variable	Support mass (g)	Pre-calcination time (h)	Pre-calcination temperature (°C)	Stirring speed (rpm)
Low level (–)	8.00	8	120	1200
High level (+)	10.00	10	140	2400

2.2. Synthesis of Fe-Ni/kaolin Catalyst

The wet impregnation method was used in the catalyst preparation. A 2^4 factorial design was employed in order that four factors were studied at two levels as described in Table 1. The varied parameters include the support mass (kaolin), pre-calcination time, pre-calcination temperature, and stirring speed. The wet impregnation technique was based on the variation of the two support mass values with the lower level being 8 g and the higher level being 10 g. The pre-calcination temperature was 120°C at the lower level and 140°C at the higher level, while the pre-calcination time was 8 h and 10 h at the lower and higher levels, respectively. The stirring speed was 1200 rpm and 2400 rpm at the lower and higher levels, respectively. The details are presented in Table 1.

The optimization of the variables that affect the catalyst yields was conducted using a factorial design (2^4 factorial design): 5.05 g of $Fe(NO_3)_3.9H_2O$ and 3.64 g of $Ni(NO_3)_2.6H_2O$ were weighed and mixed in a beaker. Thereafter, the weighed sample comprised of Fe and Ni nitrates was ground to a fine powder and later dissolved in 50 mL of distilled water to create a 0.25 M Fe-Ni (50:50 w/w) solution. This 50 mL solution was added separately to 8 g and 10 g of kaolin. The mixture was allowed to age for 30 min on a magnetic stirrer at a stirring speed of 1200 rpm and 2400 rpm. The resulting slurries were partially dried at room temperature and later oven dried at temperatures of 120°C and 140°C for 8 h and 10 h. The mixtures were later cooled to room temperature, ground, and finally screened with a 150 μm sieve. Then, the catalyst powders were calcined at 500°C for 16 h in a furnace in order to decompose the nitrates. Finally, the sample was weighed and recorded in order to determine the yield, using the relationship presented in eqs 1 and 2.

$$\textit{Catalyst Yield before calcination} = \frac{W_{\textit{Before oven drying}} - W_{\textit{After oven drying}}}{W_{\textit{Before oven drying}}} \times 100\% \quad (1)$$

$$\textit{Catalyst Yield after calcination} = \frac{W_{\textit{Before calcination}} - W_{\textit{After calcination}}}{W_{\textit{Before calcination}}} \times 100\% \quad (2)$$

2.3. Production of multi walled carbon nanotubes

The MWCNTs were synthesized using the decomposition of acetylene on a kaolin-supported bimetallic catalyst in a tubular quartz tube placed horizontally in a furnace as depicted in Fig. 1. The furnace was controlled electronically in order to ensure that the heating rate, reaction temperature, and flow rate of gas were maintained at the required rates. C_2H_2 was used as the carbon source. The catalytic chemical vapor decomposition of C_2H_2 at a temperature range of 750–800°C was conducted in a horizontal furnace in order to produce MWCNTs, at atmospheric pressure in the presence of argon as the carrier gas.

The 2^4 factorial designs at two levels as presented in Table 2 was used to investigate the effect of the reaction temperature, reaction time, argon flow rate, and acetylene flow rate on the yield of MWCNTs.

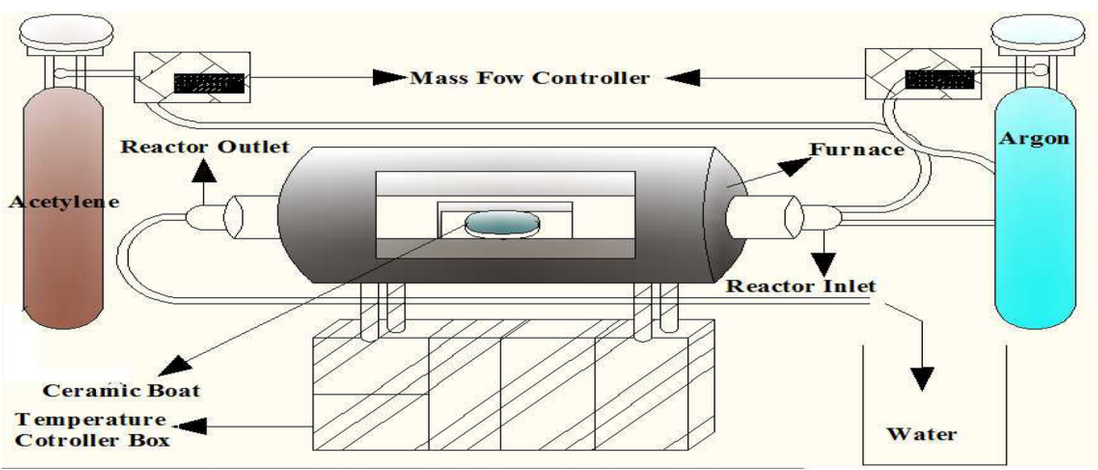

Fig. 1. Diagram of the experimental setup for the multi-walled carbon nanotubes production

Table 2. Parameter variations for the 2^4 factorial designs for the multi-walled carbon nanotube syntheses

Variable	Reaction temperature (°C)	Reaction time (min)	Ar flow rate (mL/min)	C_2H_2 flow rate (mL/min)
Low level (–)	750	45	230	150
High level (+)	800	60	280	200

One gram of the prepared catalyst was spread to form a thin layer in a quartz boat (11 × 2.6 cm) and placed at the center of the quartz tube. The furnace was heated at 10°C/min while argon (Ar) was allowed to flow at a rate of 30 mL/min in order to create an inert environment, to remove contaminants, and to prevent oxidation of the samples during the experiment. Once the desired temperature was reached (750°C and 800°C), the Ar flow rate was adjusted to 230 mL/min and 280 mL/min, respectively, for the lower and higher levels. Thereafter, the carbon source (C_2H_2) was introduced at a flow rate of 150 mL/min and 200 mL/min for the lower and higher levels, respectively. The reaction was allowed to proceed for a period of 45 min and 60 min, respectively. Subsequently, the acetylene flow was stopped and the furnace was allowed to cool to room temperature under a continuous flow of argon at a flow rate of 30 mL/min. Then, the boat containing the sample was removed from the reactor and weighed in order to determine the quantity of MWCNTs produced. The percentage of the MWCNT yield was determined using eq 3 [23].

$$MWCNTs\,Yield\,(\%) = \frac{W_{Product} - W_{catalyst}}{W_{catalyst}} \times 100\% \quad (3)$$

2.4. Purification of MWCNTs

Regarding the purification of the MWCNTs, which involved the removal of impurities such as Fe, Ni, and kaolin present in the as-produced carbon materials, the optimum sample was treated with 30% nitric acid (HNO_3) with continuous stirring on a magnetic stirrer for 3 h at room temperature. Thereafter, the mixture was refluxed and allowed to settle. Then, the mixture was filtered and washed with distilled water in order to ensure a pH of approximately 7, and it was dried at 120°C for 24 h and stored.

2.5. Characterization of Fe-Ni/kaolin catalyst and MWCNTs

The catalyst-produced, as-grown, and purified MWCNTs at the optimum conditions were characterized in order to determine its thermal stability, surface area, nature of functional groups, degree of crystallinity, and morphology using thermalgravimetric analysis (TGA; TGA 4000, Perkin Elmer, USA), Brunauer-Emmett-Teller (BET; NOVA 4200e, Quantachrome Instruments, USA), Fourier transform infrared (FT-IR; Perkin Elmer Frontier Spectrometer), X-ray diffractometer (XRD; PW 1800 diffractometer, Philips, Netherlands), high-resolution scanning electron microscope coupled with electron diffraction spectrometer (HRSEM-EDS; JEM 100S, JEOL Ltd., Japan), and high resolution transmission electron microscope (HRTEM)/selected area electron diffraction (SAED) (Philips CM20 FEG, The Netherlands).

3. Results and Discussion

3.1. Preparation of Fe-Ni/kaolin catalyst

As previously discussed in the experimental section, the four process parameters of the support mass, the pre-calcination time, the pre-calcination temperature, and the stirring speed were investigated using a 2^4 factorial experimental design. Each parameter was considered at two specified levels (upper and lower) and the results obtained are presented in Table 3. The best catalyst yield of 83.38% was obtained in experiment 15, under the optimum conditions of a support mass of 8 g, a pre-calcination time of 10 h, a pre-calcination temperature of 140°C, and a stirring speed of 2400 rpm. The reduction in the catalyst yield after calcination resulted from the multiple changes that occurred during the process, including the active phase generation, loss of chemically bound water, and changes in the pore size distribution.

3.1.1. Effect of mass of support

In Table 3, it can be seen that when the support mass was 8 g, the pre-calcination time was 8 h, the pre-calcination temperature was 120°C, and the stirring speed was 1200 rpm, the catalyst yield before calcination was 80.73%. It was found that after calcination at 500°C for 16 h, the catalyst yield reduced to 67.75%. Similarly, when the support mass was 10 g under the same experimental conditions as those at 8 g, a similar trend was observed with the catalyst yield before calcination being more than 10% greater than the catalyst yield after calcination. With the exception of experiments 1 and 2, it was found that the catalyst yield before and after calcination with 8 g of support mass was greater than when 10 g support mass was incorporated into the bimetallic catalyst (Fe-Ni) at a constant pre-calcination time, temperature, and stirring speed. Considering these results, it can be concluded that an increase in the support mass from 8 g to 10 g while maintaining the other variables constant allowed physical separation of the nanoparticles, which prevented agglomeration into larger crystallites and thus reduced the number of surface metal atoms per unit mass of metal, which consequently decreased the number of active sites of the catalyst and the catalyst yield.

3.1.2. Effect of pre-calcination time

The influence of the pre-calcination time on the catalyst yield was also investigated and the results are presented in

Table 3. Factorial design for the Fe-Ni/kaolin catalyst preparation

Experiment	Support mass (g)	Pre-calcination time (h)	Pre-calcination temperature (°C)	Stirring speed (rpm)	Catalyst yield (%)	
					Before calcination	After calcination
1	8	8	120	1200	80.73	67.75
2	10	8	120	1200	81.16	71.75
3	8	10	120	1200	81.08	68.25
4	10	10	120	1200	79.32	69.00
5	8	8	140	1200	83.23	81.24
6	10	8	140	1200	80.15	79.25
7	8	10	140	1200	83.59	81.00
8	10	10	140	1200	81.50	81.08
9	8	8	120	2400	81.78	77.50
10	10	8	120	2400	78.85	69.00
11	8	10	120	2400	81.65	70.50
12	10	10	120	2400	79.11	72.00
13	8	8	140	2400	81.66	74.25
14	10	8	140	2400	77.07	69.50
15	8	10	140	2400	84.75	83.38
16	10	10	140	2400	80.25	79.59

Table 3. The pre-calcination process is a combined mass and heat transfer problem in which the evaporation and heat transfer rate are coupled by the heat of the evaporation. The result obtained in Table 3 demonstrated the variation in the catalyst yield with two different pre-calcination times of 8 h and 10 h. For experiments 1 and 2 where the pre-calcination time was 8 h, it was found that the catalyst yields before calcination were 80.73% and 81.16%, respectively. This indicates an increment of 0.43%. With the exception of experiments 1 and 2, a decrease of 2–4% in the catalyst yield before calcination was observed irrespective of the pre-calcination time. However, the high yield of the catalyst before and after calcination was obtained at 10 h of pre-calcination time compared with 8 h. This pattern of results can be attributed to the high rate of dispersion of the active metals onto the supported substrate, and the rate of elimination of water from the pores at 10 h pre-calcination time was faster, which resulted in the increase in the concentration of precursors until saturation which increased the catalyst yield.

3.1.3. Effect of pre-calcination temperature

The influence of the pre-calcination temperature on the catalyst yield was also investigated and the results are presented in Table 3. The results depicted in Table 3 indicate that the increase in the pre-calcination temperature from 120°C to 140°C for almost all experiments before and after calcination had a noticeable effect on the catalyst yield. The most plausible reasons for these results are the large driving force and the evaporation rate during the synthesis process. It is evident from the results obtained that 140°C was sufficient for the optimum catalyst yield of 84.75% and 83.38% before and after calcination, respectively. These results were due to increases in the interactions between the support (kaolin) and the active metal (Fe-Ni) at 140°C, which accelerated the sintering and resulted in a high catalyst yield.

3.1.4. Effect of stirring speed

The importance of the stirring speed is to ensure uniform miscibility of the metal particles with the support materials in order to guarantee that all regions have the support dispersed with the active components during the synthesis process. It is evident from Table 3 that the catalyst yield after calcination increased with increases in the stirring speed from 1200 rpm to 2400 rpm when the other parameters were maintained constant. This increase in yield at a high stirring speed resulted from the filterability of the active metal (Fe-Ni) with the support, coupled with the increase in the rate of diffusion of the metal particles, which favored large depositions of metals on the pores of the support. It can be seen from the results obtained that the investigated process parameters of the support mass, pre-calcination time, pre-calcination temperature, and stirring speed significantly influence the catalyst yield.

3.1.5. Statistical analysis of the Fe-Ni/kaolin catalyst

The statistical analyses of the results obtained are presented in Table 4. It can be seen that the pre-calcination temperature significantly influenced the catalyst yield of 54.07% with a

Table 4. Effects of the factors on the preparation of the Fe-Ni/kaolin catalyst yield response

Factor	Effect	Sum of square	% Contribution	Coefficient estimate
A	–1.59	10.08	2.16	–0.795
B	1.82	13.25	2.84	0.910
C	7.94	252.23	54.07	3.970
D	–0.45	0.81	0.17	–0.225
AB	1.22	5.98	1.28	0.610
AC	–1.03	4.20	0.90	–0.515
AD	–2.30	21.11	4.52	–1.150
BC	3.38	45.77	9.81	1.690
BD	1.98	15.76	3.38	0.990
CD	–3.51	49.35	10.57	–1.755
ABC	–0.46	0.86	0.19	–0.230
ABD	1.52	9.21	1.97	0.760
ACD	0.64	1.64	0.35	0.320
BCD	2.42	23.47	5.03	1.210
ABCD	–1.80	12.89	2.76	–0.900

A, support mass; B, pre-calcination time; C, pre-calcination temperature; D, stirring speed

positive effect of 7.94. The results further demonstrated that the combination of process parameters positively influenced the catalyst yield. It should be noted that some parameters had a negative effect, which implies that increases in the values of these parameters would result in a decrease in the catalyst yield.

3.2. Characterization of the optimum Fe-Ni/kaolin catalyst yield

The catalyst obtained at the optimal conditions of a support mass of 8 g, a pre-calcination time of 10 h, a pre-calcination temperature of 140°C, and a stirring speed of 2400 rpm was characterized in order to determine its qualities. However, prior to the synthesis of the catalyst for the MWCNT growth, the support material (kaolin) was characterized using X-ray fluorescence (XRF), TGA, and BET in order to verify its suitability as a catalyst support for MWCNT production.

3.2.1. XRF analysis of kaolin

The X-ray fluorescence (XRF) analysis of the kaolin support is presented in Table 5.

The results demonstrate that the kaolin contained SiO_2 (54.21%) and Al_2O_3 (28.43%) as the major constituents with other oxides present in trace amounts. Lodya et al. [24] reported that high surface area materials such as SiO_2, Al_2O_3, TiO_2, and $CaCO_3$ provide excellent supports for catalytic MWCNT production. Based on the obtained

Table 5. Elemental composition of the Kankara kaolin

Oxide	Kaolin (wt %)
SiO_2	54.21
Al_2O_3	28.43
Fe_2O_3	0.80
TiO_2	0.11
CaO	1.86
MgO	0.41
Na_2O	0.35
K_2O	3.90
MnO	0.03
BaO	0.73
SO_3	0.22
Cr_2O_3	0.04
V_2O_5	0.10
LOI	8.81
Total	100.00

LOI: Loss of Ignition

percentage oxide composition, the locally sourced kaolin appears to be a promising alternative support to the previously used alumina (Al_2O_3), titania (TiO_2), and silica (SiO_2); furthermore, it is a less expensive support than the previously used ones.

3.2.2. TGA and DTG analysis of kaolin

Fig. 2 presents the thermal stability of the support material (kaolin). It was found that kaolin was stable from 30°C to 380.30ºC without significant loss; however, it started to decompose from 380.30°C to 573.70°C. Over this temperature range, a weight loss of 13.94% was observed; this may be ascribed to the loss of the absorbed water molecules em-

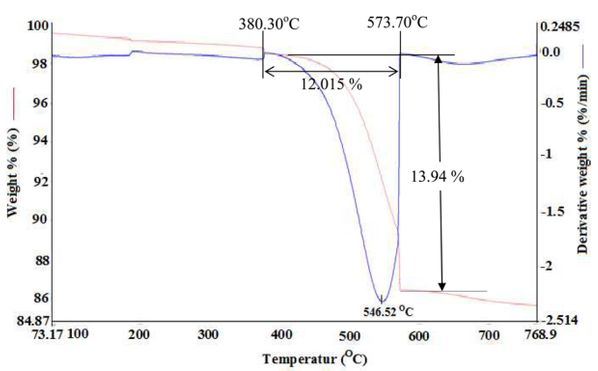

Fig. 2. TGA and DTG results for kaolin. TGA, thermal gravimetric analysis; DTG, derivative thermogravimetric analysis.

bedded in the kaolin and the volatile organic matters. The weight loss could also be related to the phase transition from a crystalline kaolinite to an amorphous metakaolin. Beyond 573.70°C, no further weight loss was observed until 768.9ºC, which indicates that the kaolin was thermally stable at this temperature. The derivative thermogravimetric analysis (DTG) exhibited only one large endothermic peak at 546.52°C.

3.2.3 TGA and DTG of optimum Fe-Ni/kaolin catalyst

The TGA/DTG profiles of the bimetallic catalyst on the kaolin support are depicted in Fig. 3.

It can be seen in Fig. 3 that there was a loss of crystallization water at 73.31–269.82°C from the two salts $Fe(NO_3)_3{\cdot}9H_2O$ and $Ni(NO_3)_2{\cdot}6H_2O$, which resulted in the formation of the anhydrous salts of $Fe(NO_3)_3$ and $Ni(NO_3)_2$. As discussed earlier in Fig. 2, kaolin was thermally stable in this temperature range. According to Fig. 3, four different decomposition stages were observed in the TGA profile: the first degradation occurred from 73.10°C to 98.93°C with a small weight loss of 0.72%. The weight loss at this temperature was attributed to the loss of the physiosorbed and chemisorbed water molecules. The second degradation stage was observed at 170–323°C with a corresponding weight loss of 6.53%. The third and fourth decomposition stages were observed at 377.92–570.71°C and 863–917°C with corresponding weight losses of 9.13% and 1.06%, respectively. The total weight loss of 17.43% before calcination was observed. However, at 481.97°C, multiple phase changes occurred due to the conversion of the anhydrous nitrate salts to their respective metallic oxides, including formation of the bimetallic oxide $NiFe_2O_4$. The detailed reaction patterns are described in eqs 4-9. At this temperature, kaolin was found to equally decompose into $2Al_2Si_2O_7$ and $4H_2O$.

$$2Al_2Sl_2O_5(OH)_4 \rightarrow 2Al_2Si_2O_7 + 4H_2O \quad (4)$$

$$Fe(NO_3)_3 .9H_2O + water \rightarrow Fe(NO_3)_3 + \uparrow 9H_2O + \uparrow water \quad (5)$$

$$Ni(NO_3)_2 .6H_2O + water \rightarrow Ni(NO_3)_2 + \uparrow 6H_2O + \uparrow water \quad (6)$$

$$Ni(NO_3)_2 \rightarrow NiO + \uparrow NO_2 + \uparrow O_2 \quad (7)$$

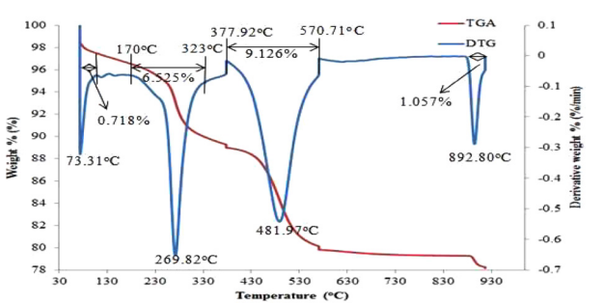

Fig. 3. TGA and DTG profiles of the Fe-Ni/kaolin catalyst before calcination. TGA, thermal gravimetric analysis; DTG, derivative thermogravimetric analysis.

$$Fe(NO_3)_3 \rightarrow Fe_2O_3 + \uparrow NO_2 + \uparrow O_2 \quad (8)$$

$$Fe_2O_3 + NiO \rightarrow NiFe_2O_4 \quad (9)$$

Fig. 4 represents the TGA and DTG profiles of Fe-Ni/kaolin after calcination at 500°C for 16 h. The weight loss of approximately 6.63% that occurred from 379.37°C to 573.33°C was attributed to the catalyst decomposition and subsequent deposition of the Ni-Fe ($NiFe_2O_4$) precursors on the kaolin support. The formation of $NiFe_2O_4$ ceased near 573.33°C and beyond, because phase transitions were not observed. This indicated that the catalyst support was thermally stable beyond this temperature.

3.2.4. BET analysis of kaolin and optimum Fe-Ni/kaolin catalyst

The BET surface area of kaolin and the developed bimetallic catalyst were determined under N_2 conditions and the results are presented in Table 6.

According to Table 6, the BET surface area, pore volume, and pore size of kaolin were 12.55 m^2/g, 0.00645 cm^3/g, and 2.064 nm, respectively. Similarly, the BET surface area, pore volume, and pore size of the Fe-Ni/kaolin catalyst were 3.76 m^2/g, 0.0019 cm^3/g, and 0.5986 nm, respectively. A decrease in the BET surface area of the catalyst was obtained after loading the Fe-Ni on the kaolin, and this indicates appropriate incorporation of the metallic particle into the pores rather than on the surface. The decrease in the surface area after impregnation might be ascribed to the structural changes of the support and not the metal ions. This BET result corroborates the XRD results.

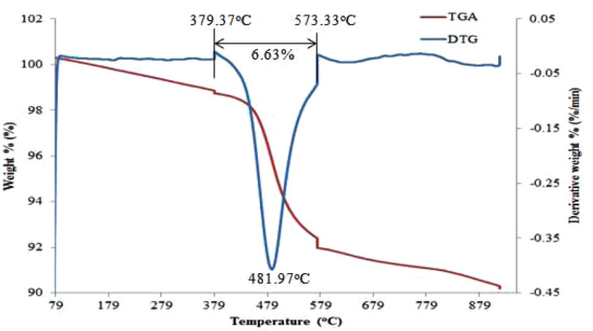

Fig. 4. TGA and DTG profiles of the Fe-Ni/kaolin catalyst after calcination. TGA, thermal gravimetric analysis; DTG, derivative thermogravimetric analysis.

Table 6. Surface area, pore volume, and pore size of kaolin and the catalyst

	Kaolin	Fe-Ni/kaolin catalyst
BET surface area ($m^2\ g^{-1}$)	12.550	3.7600
Pore volume ($cm^3\ g^{-1}$)	0.0065	0.0019
Pore size (nm)	2.064	0.5986

BET, Brunauer-Emmett-Teller.

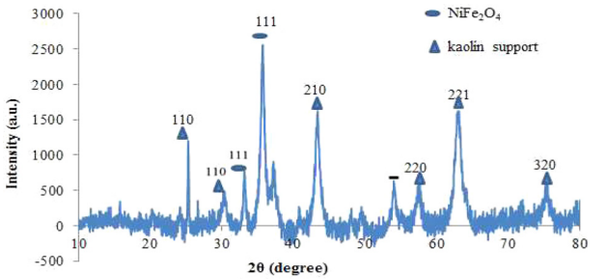

Fig. 5. X-ray diffractometer pattern for the Fe-Ni/kaolin catalyst

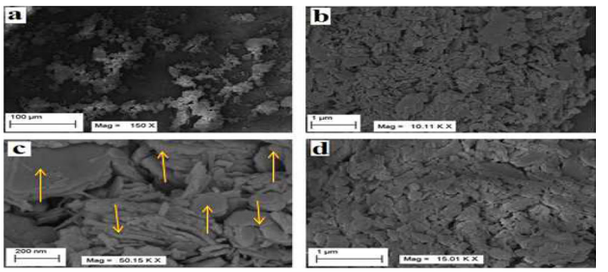

Fig. 6. The morphology of the Fe-Ni/kaolin Catalyst with an arrow indicating the encapsulated flake-like structure

3.2.5. XRD analysis of the optimum Fe-Ni/kaolin catalyst

The X-ray diffraction (XRD) pattern of the optimum synthesized Fe-Ni/kaolin catalyst after calcination is presented in Fig. 5.

The XRD pattern reveals the presence of the following sharp diffraction peaks at 2θ values of 25.32°, 30.24°, 33.15°, 35.71°, 43.42°, 57.57°, 62.98°, and 75.20°. The 2θ values at 33.15° and 35.71° represent the characteristic peaks of a crystalline bimetallic catalyst ($NiFe_2O_4$). The 2θ values at 25.32°, 30.24°, 43.42°, 57.57°, 62.98°, and 75.20° correspond to the kaolinite mineral phase. This demonstrates the extent of the crystallinity of the prepared catalyst as evident in the orderly distribution of the bimetallic ions on the pores of the support. The inter-planar spacing between the atoms (*d*-spacing) in the synthesized Fe-Ni/kaolin catalysts was calculated using eq 11.

$$d = \frac{\lambda}{2\mathrm{Sin}\theta} \quad (n = 1), \tag{11}$$

, where d is the inter-planar spacing between the atoms present in the catalyst, θ is the diffraction angle, and λ is the XRD wavelength constant, which is given as 0.1541 nm. The crystallite size of the Fe-Ni/kaolin catalyst was calculated using the Debye-Scherrer formula in eq 12 [25].

$$D = \frac{0.94\lambda}{\mathrm{FWHM}\ \mathrm{Cos}\theta}, \tag{12}$$

, where λ is the wave length of the X-ray (0.1541 nm), β is the full width at half maximum (FWHM), θ is the diffraction angle, and D is the crystallite size of the synthesized catalyst. The crystallite sizes of $NiFe_2O_4$ corresponding to the crystal plane (111) were 24.19 nm and 14.11 nm with individual *d*-spacing values of 0.27 nm and 0.25 nm, respectively. This result further confirmed the nanocrystalline nature of the $NiFe_2O_4$ supported on kaolin. It was also observed that most catalyst particle sizes were in the range of >0.1–20.0 nm, while the average particle size of the prepared catalyst (Fe-Ni/kaolin) was 20.99 nm.

3.2.6. HRSEM image of the optimum Fe-Ni/kaolin catalyst

The particle morphology of the developed catalyst after calcination was examined using HRSEM, and the results obtained at different magnifications are presented in Fig. 6.

The low magnification micrographs (Fig. 6a and b) revealed the presence of scattered and uniform oriented nanoflakes in the Fe-Ni/kaolin composite, whereas the higher magnification micrographs (Fig. 6c and d) exhibited well distributed nanoflakes grown on the substrate surface (kaolin). A close observation of the micrographs (Fig. 6b and d) revealed that the nanoflakes of the metal catalysts were maximally distributed on the surface of the kaolin support material. The random arrangement of the nanoflakes is an indication of a highly porous surface material, which is an essential requirement for a catalyst to be used in CNT synthesis.

3.2.7. HRTEM images of the optimum Fe-Ni/kaolin catalyst

The morphological structure of the prepared catalyst (Fe-Ni/kaolin) was further investigated using HRTEM, and the results are presented in Fig. 7.

It can be seen that the pore and pore walls of the prepared catalyst (Fe-Ni/kaolin) can be distinguished due to their different densities. As seen in Fig. 7a, two regions can be observed: bright regions and dark regions. Furthermore, in each region, there is the presence of the prepared catalyst particles on the supported kaolin. It can be seen that the metallic particles were adequately incorporated into the supported kaolin. The dark regions correspond to the pore wall, while the bright regions correspond to the catalyst pore. The estimated catalyst particle size was in the range of 29–31 nm. The distances of the lattice planes for the bi-metallic Fe-Ni (Fig. 7b) was measured from the lattice fringes and was 0.3 nm. The presence of the lattice fringes indicates the crystalline nature of the prepared Fe-Ni/kaolin catalyst.

3.2.8. EDX spectrum of the optimum Fe-Ni/kaolin catalyst

Qualitative and quantitative elemental analyses of the prepared catalyst particles were determined using energy dispersive X-ray (EDX) spectroscopy, and the results are presented

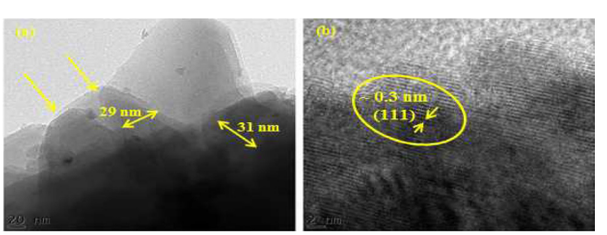

Fig. 7. High resolution transmission electron microscope image of the Fe-Ni/kaolin catalyst: (a) the arrows not some Fe-Ni nanoparticles (approximately 31 nm) supported on the kaolin after calcination and (b) the presence of a lattice-fringe pattern of approximately 0.3 nm apart.

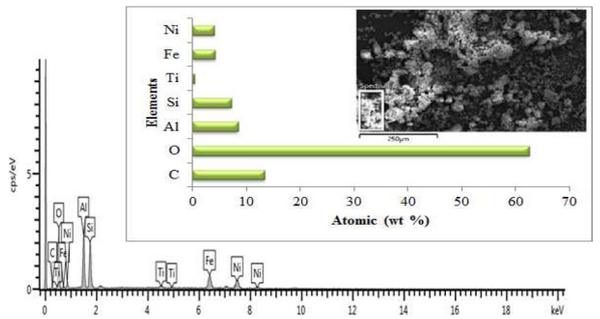

Fig. 8. Energy dispersive X-ray spectrum of the Fe-Ni/kaolin catalyst

in Fig. 8

It can be seen that the prepared catalyst particles contained different elements such as Fe, Ni, Ti, Si, Al, O, and C in different proportions. The elements Ti, Si, and Al possibly originated from the supported kaolin. Fe and Ni were obtained from their respective salts, while C came from the holey carbon grid. This result also demonstrates that the particles contained both Fe and Ni in a 1:1 wt% ratio (50:50), which agreed well with the chosen stoichiometry during the preparation of the catalyst. Thus, the average atomic ratio of Ni to Fe was almost 1:1, which indicates that a pure $NiFe_2O_4$ was synthesized.

3.3.0. Effect of Reaction Temperature

It has been reported that temperature has a significant function in MWCNT growth using the CCVD method in a CVD reactor. Based on this, the results obtained for the effect of temperature variations in the range of 750–800°C on the production rate of MWCNTs is presented in (Fig. 9). In the

Table 7. As-prepared MWCNT mass using the 2^4 factorial design

Run	Reaction temperature (°C)	Reaction time (min)	Argon flow rate (mL/min)	Acetylene flow rate (mL/min)	As-prepared MWCNT yield (%)
1	750	45	230	150	210
2	800	45	230	150	178
3	750	60	230	150	240
4	800	60	230	150	178
5	750	45	280	150	195
6	800	45	280	150	151
7	750	60	280	150	224
8	800	60	280	150	177
9	750	45	230	200	235
10	800	45	230	200	190
11	750	60	230	200	306
12	800	60	230	200	204
13	750	45	280	200	214
14	800	45	280	200	153
15	750	60	280	200	256
16	800	60	280	200	184

MWCNT, multi-walled carbon nanotubes.

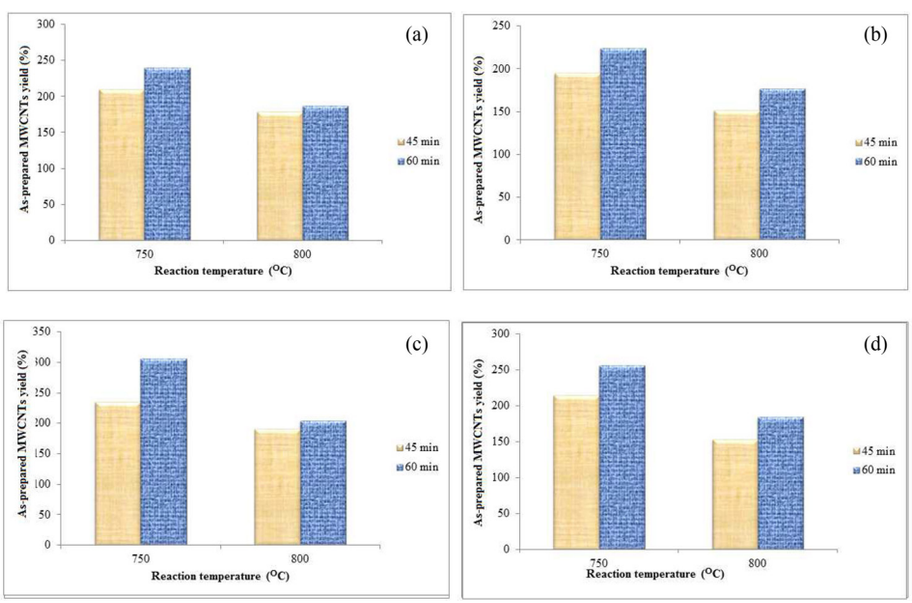

Fig. 9. Effect of the reaction temperature on the as-prepared multi-walled carbon nanotube (MWCNT) yield: (a) Ar flow rate of 230 mL/min and C_2H_2 flow rate of 150 mL/min; (b) Ar flow rate of 280 mL/min and C_2H_2 flow rate of 150 mL/min; (c) Ar flow rate of 230 mL/min and C_2H_2 flow rate of 200 mL/min; and (d) Ar flow rate of 280 mL/min and C_2H_2 flow rate of 200 mL/min.

Fig. 9 depict a decrease in the MWCNT yield as the temperature increased. The decrease in the MWCNT yield at 800°C could be attributed to the low decomposition of the acetylene over the catalyst.

3.3.1. Effect of Reaction Time

The effect of the reaction time on the MWCNT yields between 45 min and 60 min was investigated and the results are presented in Fig. 10. It can be seen from Fig. 10 that, at a constant production temperature, the MWCNT yield obtained at 60 min of production time was higher than that obtained at 45 min. The potential cause of the high MWCNT yield at 60 min is the essential equilibrium between the acetylene (feedstock) and the surface of the active points of the prepared catalyst particles, which resulted in the total decomposition of the acetylene. Moreover, the low MWCNT yield at 45 min may result from the low residence time of the acetylene in the CVD reactor, which could lead to the incomplete decomposition of acetylene.

3.3.2. Effect of Argon Flow Rate

The results obtained for the effect of the argon flow rate on the MWCNT yield at a constant acetylene flow rate, reaction

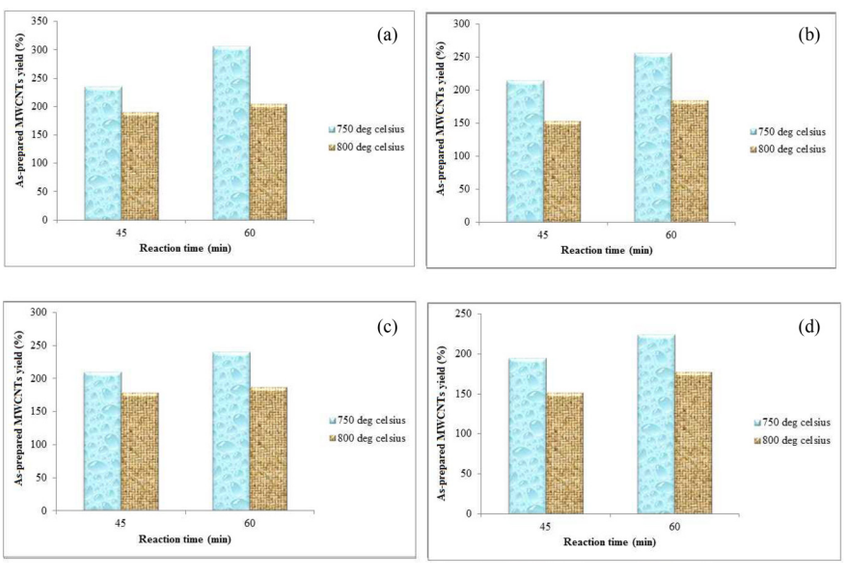

Fig. 10. Effect of the reaction time on the as-prepared multi-walled carbon nanotube (MWCNT) yield: (a) Ar flow rate of 230 mL/min and C_2H_2 flow rate of 150 mL/min; (b) Ar flow rate of 280 mL/min and C_2H_2 flow rate of 150 mL/min; (c) Ar flow rate of 230 mL/min and C_2H_2 flow rate of 200 mL/min; and (d) Ar flow rate of 280 mL/min and C_2H_2 flow rate of 200 mL/min.

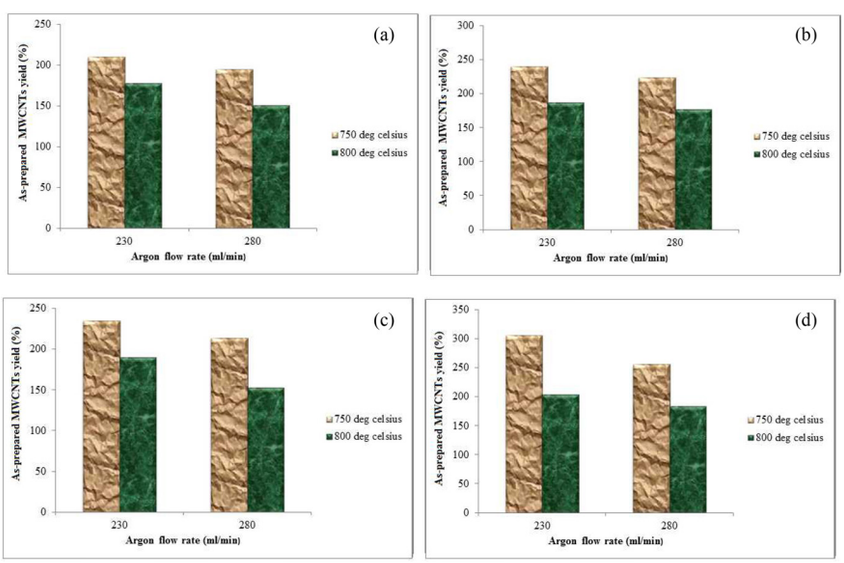

Fig. 11. Effect of the argon flow rate on the as-prepared multi-walled carbon nanotube (MWCNT) yield: (a) reaction time of 45 min and C_2H_2 flow rate of 150 mL/min; (b) reaction time of 60 min and C_2H_2 flow rate of 150 mL/min; (c) reaction time of 45 min and C_2H_2 flow rate of 200 mL/min; and (d) reaction time of 60 min and C_2H_2 flow rate of 200 mL/min

DOI: http://dx.doi.org/10.5714/CL.2017.21.033

time, and reaction temperature are presented in Fig. 11 and Table 7. According to Fig. 11, as the Ar flow rate increased from 230 mL/min to 280 mL/min, the production rate of the CNTs decreased. A potential explanation for this is that, at 230 mL/min, the Ar carried sufficient acetylene into the reaction zone and it required a longer time to decompose and deposit on the catalysts for MWCNT formation. However, at 280 mL/min, most acetylene escaped via the CVD reactor outlet due to the high velocity profile created by Ar; therefore, the acetylene could not be deposited on the catalyst and is thus responsible for the small formation of MWCNTs.

3.3.3. Effect of Acetylene Flow Rate

The production rate of MWCNTs is directly proportional to the acetylene flow rate at various decomposition temperatures, reaction times, and argon flow rates. The results of the effect of the C_2H_2 flow rate on the MWCNT yield is presented in Fig. 12. It can be seen from Fig. 12 that the MWCNT yield increased with increases in the acetylene flow rate from 150 mL/min to 200 mL/min for all experiments. This might be attributed to the high concentration of C_2H_2 in the CVD reaction zone with a high velocity profile created by the high flow rate. This aids in the formation of the required MWCNTs via induction of acetylene at a faster rate into the reaction zone of the CVD reactor for decomposition into the MWCNTs than at a lower flow rate.

3.3.4. Comparison of the MWCNTs yield results of previous and present study

Table 8 presents a comparison of the MWCNT yields in this study with those of previous studies. The present study exhibits a remarkable improvement in the MWCNT yield.

The comparison of this present study with previous works in terms of MWCNT yields as presented in Table 8 indicates that the MWCNT yield depends on the type of active phase, the nature of the catalyst support, and the conditions of the MWCNT production. The higher MWCNT yield obtained in this study compared with previous studies might be linked to the nature of the support material. According to the XRF results in Table 5, several metal oxides are embedded within the kaolin framework. Thus, the higher MWCNT yield in this study can be ascribed to the combination of oxides embedded in kaolin compared with the individual support oxides reported in the literature. Notably, a significant factor influencing the catalyst activity during the MWCNT production is the size of the metallic particles, which depend on the nature of the support and metal-support interaction. Therefore, the higher MWCNT yield observed in this work can be linked to the higher metal dispersion of the kaolin-supported catalyst. Another important reason for the significant improvement of the MWCNT yield is due to differences in the MWCNT synthesis conditions as described in Table 8.

3.3.5. Statistical analysis of MWCNTs yield

Furthermore, the data obtained from the as-prepared MWCNT yield in Table 4 were later subjected to regression analyses using Minitab 16.10 software (Minitab Inc, USA) in order to estimate the effects of the synthesis variables. The analysis of variance (ANOVA) of the yield of the as-prepared MWCNTs (%) is summarized in Tables 9 and 10.

The coded mathematical model for the 2^4 factorial designs is provided in eq 13.

$$MWCNTs\,Yield(\%) = X_0 + X_1A + X_2B + X_3C + X_4D + X_5AB + X_6AC + X_7AD + X_8BC + X_9BD + X_{10}CD + X_{11}ABC + X_{12}ABD + X_{13}ACD + X_{14}BCD + X_{15}ABCD, \quad (13)$$

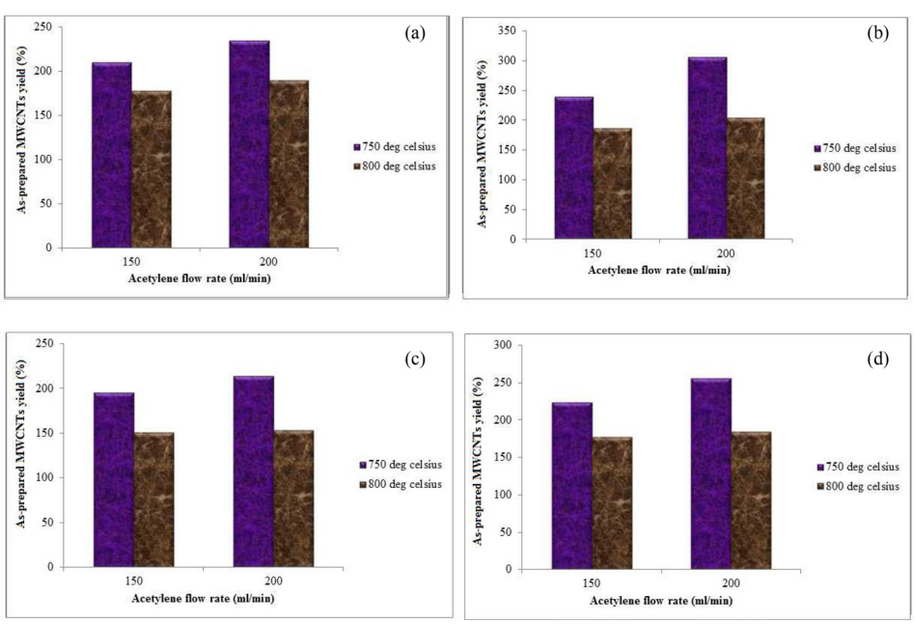

Fig. 12. Effect of the acetylene flow rate on the as-prepared multi-walled carbon nanotube (MWCNT) yield: (a) reaction time of 45 min and Ar flow rate of 230 mL/min; (b) reaction time of 60 min and Ar flow rate of 230 mL/min; (c) reaction time of 45 min and Ar flow rate of 280 mL/min; and (d) reaction time of 60 min and Ar flow rate of 280 mL/min

Table 8. Comparison of the MWCNT yield results of previous studies and the present study

Catalyst	Conditions of MWCNT production	MWCNT yield (%)	Reference
Co-Ni/SiO_2	Reaction temperature: 700°C Reaction time: 60 min Hydrogen flow rate: 110 mL/min Acetylene/nitrogen mixture flow rate: 220 mL/min	9.1	[26]
Fe-Ni/SiO_2	Reaction temperature: 700°C Reaction time: 60 min Hydrogen flow rate: 110 mL/min Acetylene/nitrogen mixture flow rate: 220 mL/min	47.3	[26]
Fe-Co/SiO_2	Reaction temperature: 700°C Reaction time: 60 min Hydrogen flow rate: 110 mL/min Acetylene/nitrogen mixture flow rate: 220 mL/min	61.8	[26]
Co-Ni/γ-Al_2O_3	Reaction temperature: 700°C Reaction time: 60 min Hydrogen flow rate: 110 mL/min Acetylene/nitrogen mixture flow rate: 220 mL/min	76.4	[26]
Fe-Ni/γ-Al_2O_3	Reaction temperature: 700°C Reaction time: 60 min Hydrogen flow rate: 110 mL/min Acetylene/nitrogen mixture flow rate: 220 mL/min	239.1	[26]
Fe-Co/γ-Al_2O_3	Reaction temperature: 700°C Reaction time: 60 min Hydrogen flow rate: 110 mL/min Acetylene/nitrogen mixture flow rate: 220 mL/min	263.6	[26]
Fe-Ni/Kaolin	Reaction temperature: 750°C Reaction time: 60 min Argon flow rate: 230 mL/min Acetylene flow rate: 200 mL/min	306	Current work

Table 9. Effects of the growth factors on the MWCNT synthesis yield responses

Factor	Effect	Sum of square	% Contribution	Coefficient estimate
A	–57.00	12996	55.11	–28.50
B	32.50	3969	16.83	16.25
C	–24.50	2401	10.18	–12.25
D	22.50	2025	8.59	11.25
AB	–11.50	529	2.24	–5.75
AC	1.00	4	0.017	0.50
AD	–13.00	676	2.87	–6.50
BC	0.50	1	4.241×10^{-3}	0.25
BD	8.00	256	1.09	4.00
CD	–7.50	225	0.95	–3.75
ABC	8.00	256	1.09	4.00
ABD	–5.50	121	0.51	–2.75
ACD	2.50	25	0.11	1.25
BCD	–3.50	49	0.21	–1.75
ABCD	3.50	49	0.21	1.75

MWCNT, multi-walled carbon nanotubes; A, reaction temperature; B, reaction time; C, argon flow rate; D, acetylene flow rate.

Table 10. Summary of the analysis of variance for the multi-walled carbon nanotubes synthesis yield responses

Factor	Sum of square	Degree of freedom	Mean square	*F*-value	*P*-value[a)]
Model	23,082	10	2308.20	23.08	0.0014
A	12,996	1	12996.00	129.96	<0.0001
B	3969	1	3969.00	39.69	0.0015
C	2401	1	2401.00	24.01	0.0045
D	2025	1	2025.00	20.25	0.0064
AB	529	1	529.00	5.29	0.0698
AC	4	1	4.00	0.04	0.8494
AD	676	1	676.00	6.76	0.0482
BC	1	1	1.00	0.01	0.9242
BD	256	1	256.00	2.56	0.1705
CD	225	1	225.00	2.25	0.1939
Residual	500	5	100.00	-	-
Corrected total	23,582	15	-	-	-

R^2 = 0.9788; adjusted R^2 = 0.9364; predicted R^2 = 0.7829; Adeq. precision = 17.066.
[a)]Prob >F.

, where X_0 is the global mean, X_i is the regression coefficients, and A, B, C, D are the four operating parameters of reaction temperature, reaction time, argon flow rate, and acetylene flow rate, respectively. Through substituting the coefficients X_i in eq 13 with their respective values, eq 13 becomes eq 14:

$$MWCNTs\,Yield(\%) = +206.5 - 28.5 \times A + 15.75 \times B - 12.25 \times C + 11.25 \times D - 5.75 \times AB + 0.5 \times AC - 6.5 \times AD + 0.25 \times BC + 4 \times BD - 3.75 \times CD + 4 \times ABC - 2.75 \times ABD + 1.25 \times ACD - 1.75 \times BCD + 1.75 \times ABCD \quad (14)$$

Based on the ANOVA results presented in Table 10, A, B, C, and D were considered to be significant parameters, while AB and AD were moderately significant. In contrast, AC, BC, BD, CD, ABC, ABD, ACD, BCD, and ABCD were considered insignificant. Similarly, the Pareto chart and the normal plot of the standardized effects in Fig. 13 also confirms the result in Table 10.

The Pareto chart (Fig. 13) displays the absolute value of the effects and draws a reference line on the chart at the t-value limit (where t is the (1 - α/2) quartile of a t-distribution) with 2.57 degrees of freedom for the error term. Any effect that extends beyond this reference line was considered statistically significant. According to Fig. 13, A, B, C, D, and AD were significant based on their values being greater than or above the reference line. Furthermore, the p-value was less than 0.05 as depicted in the ANOVA results presented in Table 10. Therefore, considering the significant importance of A, B, C, D, and AD, eq 14 was reduced to eq 15, which is the final equation in terms of coded factors, as follows.

$$Y_{MWCNTs}(\%) = +206.5 - 28.5 \times A + 16.25 \times B - 12.25 \times C + 11.25 \times D - 6.5 \times AD \quad (15)$$

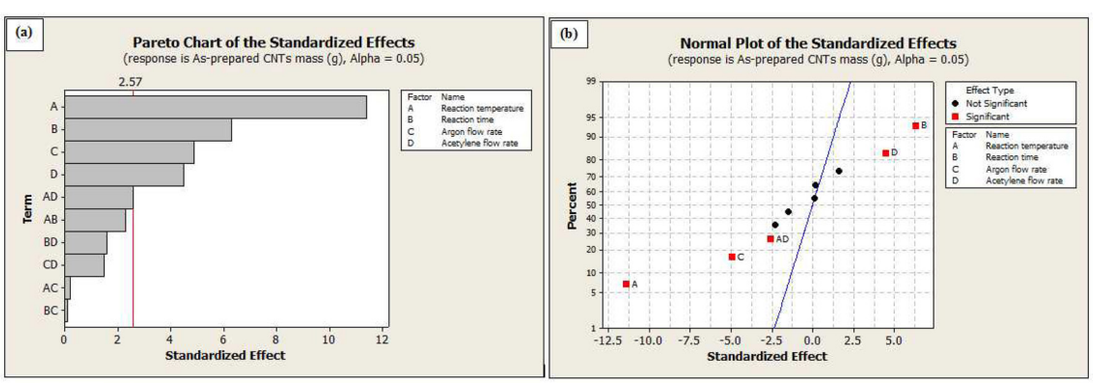

Fig. 13. (a) Pareto chart of the standardized effects and (b) normal plot of the standardized effects of the as-prepared multi-walled carbon nanotube (MWCNT) yield

Table 11. Effects of the growth factors on the MWCNT synthesis yield response

Experiment	A	B	C	D	As-prepared MWCNT yield (%)	Predicted MWCNT yield (%)	Residual
1	–	–	–	–	210	213.75	3.75
2	+	–	–	–	178	169.75	-8.25
3	–	+	–	–	240	245.25	5.25
4	+	+	–	–	187	201.25	14.25
5	–	–	+	–	195	189.25	-5.75
6	+	–	+	–	151	145.25	-5.75
7	–	+	+	–	224	220.75	-3.25
8	+	+	+	–	177	176.75	-0.25
9	–	–	–	+	235	249.25	14.25
10	+	–	–	+	190	179.25	-10.75
11	–	+	–	+	306	280.75	-25.25
12	+	+	–	+	204	210.75	6.75
13	–	–	+	+	214	224.75	10.75
14	+	–	+	+	153	154.75	1.75
15	–	+	+	+	256	256.25	0.25
16	+	+	+	+	184	186.25	2.25

MWCNT, multi-walled carbon nanotubes.

The *R*-square values of 97.88% demonstrated that this polynomial model provides very good descriptions of the relationship among the four factors and responses. This model equation was developed in order to establish the relationship between the variables investigated and the as-prepared MWCNT yield. The predicted simulated as-prepared MWCNT yield was in close agreement with the experimental MWCNT yield (Table 11).

3.4. Characterisation of MWCNTs

The prepared MWCNTs obtained with the optimum conditions (experiment 11) using the optimum Fe-Ni/kaolin catalyst were characterized and the results obtained are presented as follows.

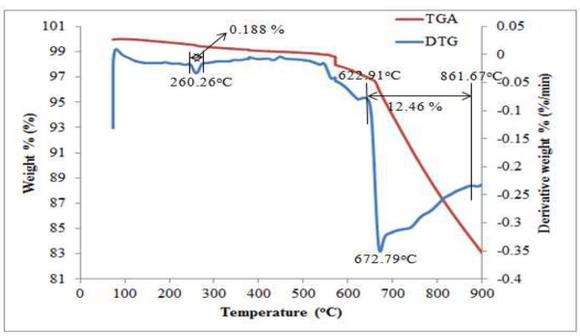

Fig. 14. TGA and DTG profiles of the as-prepared optimum multi-walled carbon nanotubes (MWCNTs). TGA, thermal gravimetric analysis; DTG, derivative thermogravimetric analysis.

3.4.1. TGA/DTG of the as-prepared and purified optimum MWCNTs

Fig. 14 represents the TGA and DTG profiles of the produced optimum MWCNTs.

According to Fig. 14, two different degradation temperatures were apparent. The first decomposition stage occurred at 230.83–269.91°C with a corresponding weight loss of 0.19%. The weight loss might be linked to the residual catalyst or oxidation products of the support material in the MWCNTs. However, the remaining 99.81% of the samples were considered to be carbonaceous materials. No significant weight loss was observed before 622.91°C in the as-grown MWCNTs, thus eliminating the presence of a significant amount of amorphous carbon. In the degradation temperature range of 622.91–861.67°C, a 12.46% weight loss was observed. This temperature range represents the decomposition profile of a typical multiwall carbon nanotube (MWCNT) with a small sharp peak in the derivative curve at 672.79ºC as depicted in Fig. 14. The 12.46% weight loss at the higher temperature demonstrated the oxidation of the MWCNTs, which was linked to the presence of graphitized carbon. Moreover, the TGA/DTG profile of the purified MWCNTs with the optimum values is presented in Fig. 15. It was found that after refluxing in NaOH and HNO_3 for 3 h, a decrease in the impu-

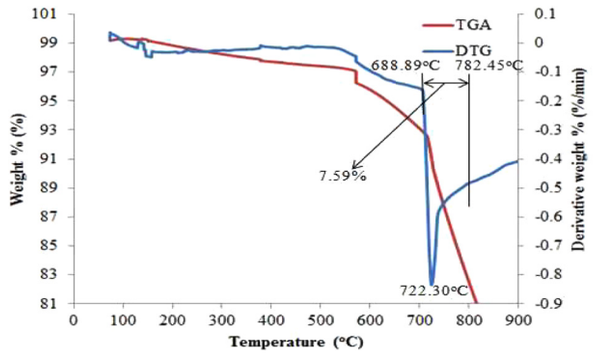

Fig. 15. TGA and DTG profiles of the purified optimum multi-walled carbon nanotubes (MWCNTs). TGA, thermal gravimetric analysis; DTG, derivative thermogravimetric analysis.

rity content was observed, which signified the effectiveness of the adopted purification process.

The derivative peak breadth exhibited an increase in the number of defects upon oxidation. The thermal stability and decomposition temperature of the MWCNTs increased from 672.79°C to 722.30°C after purification. Only 7.59% weight loss was observed at a degradation temperature range of 688.89–782.45°C. This improvement in the thermal stability could be attributed to the removal of the catalyst known to promote the oxidation of carbon.

3.4.2. BET analysis of as-prepared and purified optimum MWCNTs

The BET surface area and pore volume of the as-prepared and purified optimum MWCNTs were determined under N_2 conditions, and the results obtained are presented in Table 12.

The BET surface area, pore volume, and size of the as-prepared optimum MWCNTs were 244.4 $m^2\ g^{-1}$, 0.086 $cm^3\ g^{-1}$, and 3.04 nm, respectively. However, after purification, the BET surface area, pore volume, and pore size were slightly increased to 268.40 $m^2\ g^{-1}$, 0.105 $cm^3\ g^{-1}$, and 3.287 nm, respectively. These slight increments were linked to the successful removal of the residual catalyst and some other impurities that blocked the pores from of the as-prepared optimum MWCNT caps.

3.4.3. XRD patterns of optimum MWCNTs

The X-ray diffraction (XRD) patterns of the as-prepared and purified MWCNTs is presented in Fig. 16

The XRD patterns in Fig. 16 exhibit major peaks around 2θ = 26° and 44°, which correspond to the crystal planes (002) and (100), respectively. The two diffraction peaks, which are denoted with "C", represent the characteristic planes of a typical graphitized carbon of the CNTs. The other peaks appearing at 30.49°, 52.68°, and 61.80° with crystal planes of (110), (220), and (211), respectively, indicate the presence of kaolin. The presence of the diffraction peak near 34.88° with the corresponding crystal plane (111) indicated the presence of a bimetallic oxide ($NiFe_2O_4$), which corroborates the TGA result in Fig. 3. Furthermore, the crystal size, inter-plane distance (*d*-spacing), average particle size, and line broadening (FWHM) were calculated using Bragg's equation and the Debye-Scherrer equation. An increase in the particle size of the MWCNTs after purification from 38.84 nm to 51.25 nm was noticed. This observable increase in the particles resulted from the removal of residual metal particles from the pores of the as-prepared MWCNT. Moreover, the calculated interlayer spacings for the as-prepared and purified MWCNTs were found to be of 0.3442 and 0.3449, respectively. These values were closely related to that of graphite (0.335 nm). This further confirmed the graphitic nature of the MWCNT peaks and the significant improvement in the order of crystallinity of the MWCNTs after purification.

Table 12. Textural properties of the as-prepared and purified optimum MWCNTs

	As-prepared MWCNTs	Purified MWCNTs
BET surface area ($m^2\ g^{-1}$)	244.40	268.40
Pore volume ($cm^3\ g^{-1}$)	0.086	0.105
Pore size (nm)	3.040	3.287

MWCNT, multi-walled carbon nanotubes; BET, Brunauer-Emmett-Teller.

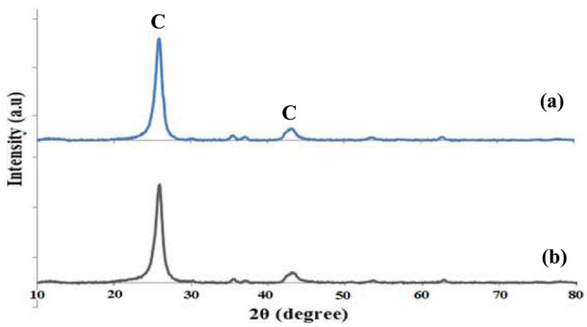

Fig. 16. X-ray diffraction patterns at the optimum multi-walled carbon nanotubes (MWCNTs): (a) as-prepared and (b) purified.

3.4.4. HRSEM analysis of as-prepared and purified optimum MWCNTs

It is evident from the various analyses conducted on the as-prepared optimum MWCNTs that impurities such as catalyst metal particles, support materials, and amorphous carbon, are present on the surface of MWCNTs. The presence of such impurities affects its morphological arrangement for different applications; hence, the need to remove these impurities was demonstrated. Fig. 17 present the HRSEM image of the as-prepared

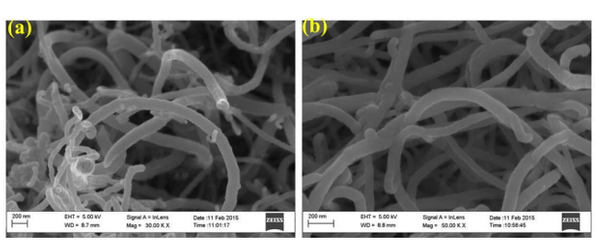

Fig. 17. High resolution scanning electron microscope micrographs of the optimum multi-walled carbon nanotubes (MWCNTs): (a) as-prepared and (b) purified

and purified optimum MWCNTs, respectively.

The HRSEM image in Fig. 17a exhibits a slight degree of agglomeration with some bright spots, which corresponds to the residual metal particle and compared with Fig. 17b, which exhibits a clear defined tubular morphology.

3.4.5. EDX analysis of as-prepared and purified optimum MWCNTs

EDX spectroscopy was used to investigate the presence of elements in the as-prepared and purified optimum MWCNTs. Table 14 reveals the presence of carbon in the samples.

Table 13 reveals the presence of elements in different proportions. The predominant deposit was carbonaceous materials which increased from 91.73 wt% to 95.02 wt% after purification. Other elements such as aluminum (Al), silicon (Si), and titanium (Ti) were detected and could possibly originate from the support materials (kaolin). The presence of iron (Fe), nickel (Ni), and oxygen (O) observed in the results were from the catalyst metal particles and were considerably reduced after purification. The copper (Cu) presences in the sample originated from the holey copper grid used during the EDX analysis.

3.4.6. HRTEM analysis of the as-prepared and purified optimum MWCNTs

A HRTEM micrograph of the as-prepared and purified optimum MWCNTs is depicted in Fig. 18a and b, respectively.

The HRTEM image clearly depicts the partition or existence of the wall. The diameter of the as-prepared MWCNT was 61 nm with the presence of an encapsulated catalyst as indicated by the arrow in Fig. 18a. After purification, there was a partial disappearance of the black spot and a decrease in the diameter to 57 nm. The partial disappearance of the black spot might be linked to the purification treatment..

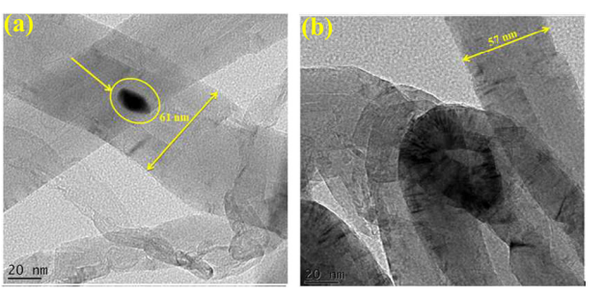

Fig. 18. High resolution transmission electron microscope images of the optimum multi-walled carbon nanotubes (MWCNTs): (a) as-prepared and (b) purified with the arrows indicating the diameter of the outer surface of the long tubes.

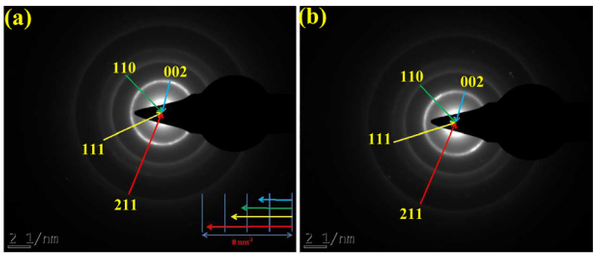

Fig. 19. Selected area electron diffraction patterns of the optimum multi-walled carbon nanotubes (MWCNTs): (a) as-prepared and (b) purified

3.4.7. SAED analysis of the as-prepared and purified optimum MWCNTs

The SAED pattern presented in Fig. 19 exhibits the strong diffraction rings for the (002) and (110) diffractions, and a pair of weak rings for the (111) and (211) diffractions.

The presence of diffuse haloes and sharp rings might originate from the amorphous carbon film on the copper grid and the MWCNTs. Using the reciprocal lattice spacings (1/d) measured from the ring occurrences, the interplanar distance (d) was determined. The interplanar spacing values were calculated from Bragg's diffraction equation using the diffraction ring diameter and the camera length of the HRTEM. The calculated interlayer spacing of approximately 0.33 nm, which corresponds to the (002) distance of the graphite carbon, agrees with the literature value.

4. Conclusions

In summary, a bimetallic catalyst (Fe-Ni) supported on kaolin was used to grow MWCNTs using the CCVD method. The influence of the support mass, pre-calcination time, pre-calcination temperature, and stirring speed on the yield of the as-prepared catalyst and MWCNTs were investigated. Based on this study, the following conclusions were drawn. The optimum catalyst yield of 83.38% was obtained at the following optimal conditions: a support mass of 8 g, a pre-calcination time of 8 h, a pre-calcination temperature of 140°C, and a stirring speed of 2400 rpm. Statistical ANOVA demonstrated that the pre-calcination temperature had a more significant effect on the catalyst yield than the other factors. The prepared catalyst exhibited high metal-support interactions between Fe-Ni and the kaolin support, which promotes the catalytic properties for the subsequent growth of the MWCNTs. The optimum yield of 306% was obtained under the optimum conditions: 750°C reaction temperature, 60 min reaction time, 230 mL/min Ar flow rate, and 200

Table 13. EDX analysis normalized to 100% of as-prepared and purified optimum MWCNTs

Optimum MWCNTs	Elemental composition (wt%)								Total (%)
	C	O	Al	Si	Ti	Fe	Ni	Cu	
As-prepared	91.73	3.44	1.57	1.48	0.08	0.89	0.72	0.11	100
Purified	95.02	1.11	0.92	1.17	0.04	0.89	0.71	0.13	100

EDX, energy dispersive X-ray; MWCNT, multi-walled carbon nanotubes.

mL/min C_2H_2. The temperature, time, argon flow rate, acetylene, and a combined effect (temperature and acetylene flow rate) contributed significantly to the higher yield of MWCNTs compared with the other factors. The simulation of the developed linear regression model exhibited close proximity to the experimental value with the predicted MWCNTs yield values. The HRTEM/SAED, HRSEM/EDX, XRD, BET, and TGA of the as-grown MWCNTs revealed that the prepared sample was a high-quality MWCNT containing fewer defects. This study demonstrated for the first time that MWCNTs can be successfully prepared from a bimetallic catalyst (Fe-Ni) supported on locally available kaolin.

Conflict of Interest

No potential conflict of interest relevant to this article was reported.

Acknowledgements

Support was received from the Tertiary Education Trust Fund (TETFUND) of Nigeria under grant number TETFUND/FUTMINNA/2014/025; this is highly appreciated. The Centre for Genetic Engineering and Biotechnology (CGEB) FUTMinna is also thanked for enabling direct access to the center facilities. The authors are grateful to the following people that helped analyzed the samples: Dr. Remy Bucher (XRD, iThemba Labs), Dr. Franscious Cummings (HRTEM, Physics Department, University of Western Cape (UWC), South Africa), and Adrian Joseph (HRSEM, Physics department, UWC, South Africa).

References

[1] Iijima S. Helical microtubules of graphitic carbon. Nature, **354**, 56 (1991). https://doi.org/10.1038/354056a0.

[2] Yang X, Zou T, Shi C, Lie E, He C, Zhao N. Effect of carbon nanotube (CNT) content on the properties of in-situ synthesis CNT reinforced Al composites. Mater Sci Eng A, **660**, 11 (2016). https://doi.org/10.1016/j.msea.2016.02.062.

[3] Voelskow K, Becker MJ, Xia W, Muhler M, Turek T. The influence of kinetics, mass transfer and catalyst deactivation on the growth rate of multiwalled carbon nanotubes from ethane on a cobalt-based catalyst. Chem Eng J, **244**, 68 (2014). https://doi.org/10.1016/j.cej.2014.01.024.

[4] Hutchison JL, Kiselev NA, Krinichnaya EP, Krestinin AV, Loutfy RO, Morawsky AP, Muradyan VE, Obraztsova ED, Sloan J, Terekhov SV, Zakharov DN. Double-walled carbon nanotubes fabricated by a hydrogen arc discharge method. Carbon, **39**, 761 (2001). https://doi.org/10.1016/S0008-6223(00)00187-1.

[5] Tombros N, Buit L, Arfaoui I, Tsoufis T, Gournis D, Trikalitis PN, van der Molen SJ, Rudolf P, van Wees BJ. Charge transport in a single superconducting tin nanowire encapsulated in a multiwalled carbon nanotube. Nano Lett, **8**, 3060 (2008). https://doi.org/10.1021/nl080850t.

[6] Tsoufis T, Jankovic L, Gournis D, Trikalitis PN, Bakas T. Evaluation of first-row transition metal oxides supported on clay minerals for catalytic growth of carbon nanostructures. Mater Sci Eng B, **152**, 44 (2008). https://doi.org/10.1016/j.mseb.2008.06.029.

[7] Maccallini E, Tsoufis T, Policicchio A, La Rosa S, Caruso T, Chiarello G, Colavita E, Formoso V, Gournis D, Agostino RG. A spectro-microscopic investigation of Fe–Co bimetallic catalysts supported on MgO for the production of thin carbon nanotubes. Carbon, **48**, 3434 (2010). http://dx.doi.org/10.1016/j.carbon.2010.05.039.

[8] Shah KA, Tali BA. Synthesis of carbon nanotubes by catalytic chemical vapour deposition: a review on carbon sources, catalysts and substrates. Mater Sci Semicond Process, **41**, 67 (2016). https://doi.org/10.1016/j.mssp.2015.08.013.

[9] Lee CJ, Lyu SC, Kim HW, Park CY, Yang CY. Large-scale production of aligned carbon nanotubes by the vapour phase method. Chem Phys Lett, **359**, 109 (2002). https://doi.org/10.1016/S0009-2614(02)00648-6.

[10] Yang X, Wu D, Chen X, Fu R. Nitrogen-enriched nanocarbons with a 3-D continuous mesopore structure from polyacrylonitrile for supercapacitor application. J Phys Chem C, **114**, 8581 (2010). https://doi.org/10.1021/jp101255d.

[11] Dai L, Patil A, Gong X, Guo Z, Liu L, Liu Y, Zhu D. Aligned nanotubes. ChemPhysChem, **4**, 1150 (2003). https://doi.org/10.1002/cphc.200300770.

[12] Yardimci AI, Yılmaz S, Selamet Y. The effects of catalyst pretreatment, growth atmosphere and temperature on carbon nanotube synthesis using Co–Mo/MgO catalyst. Diamond Relat Mater, **60**, 81 (2015). https://doi.org/10.1016/j.diamond.2015.10.025.

[13] Chiwaye N, Jewell LL, Billing DG, Naidoo D, Ncube M, Coville NJ. Insitu powder XRD and Mössbauer study of Fe–Co supported on $CaCO_3$. Mater Res Bull, **56**, 98 (2014). https://doi.org/10.1016/j.materresbull.2014.04.065.

[14] Liu WW, Chai SP, Mohamed AR, Hashim U. Synthesis and characterization of graphene and carbon nanotubes: a review on the past and recent developments. J Ind Eng Chem, **20**, 1171 (2014). https://doi.org/10.1016/j.jiec.2013.08.028.

[15] Milone C, Piperopoulos E, Lanza M, Santangelo S, Malara A, Mastronardo E, Galvagno S. Influence of the cobalt phase on the highly efficient growth of MWCNTs. Nanomater Nanotechnol, **4**, 1 (2014). https://doi.org/10.5772/58457.

[16] Jeong SW, Son SY, Lee DH. Synthesis of multi-walled carbon nanotubes using Co–Fe–Mo/Al_2O_3 catalytic powders in a fluidized bed reactor. Adv Powder Technol, **21**, 93 (2010). https://doi.org/10.1016/j.apt.2009.10.008.

[17] Schmidt DF, du Fresne von Hohenesche C, Weiss A, Schädler V. Colloidal gelation as a general approach to the production of porous materials. Chem Mater, **20**, 2851 (2008). https://doi.org/10.1021/cm7036603.

[18] Mhlanga SD, Coville NJ. Iron–cobalt catalysts synthesized by a reverse micelle impregnation method for controlled growth of carbon nanotubes. Diamond Relat Mater, **17**, 1489 (2008). https://doi.org/10.1016/j.diamond.2008.01.049.

[19] Dervishi E, Li Z, Xu Y, Saini V, Watanabe F, Biris AR, Bonpain A, Garbay JJ, Meriet A, Richard M, Biris AR. (2009) The influence of Fe–Co/MgO catalyst composition on the growth properties of carbon nanotubes. Part Sci Technol, **27**, 222 (2009). https://doi.org/10.1080/02726350902921848.

[20] Mhlanga SD, Mondal KC, Carter R, Witcomb MJ, Coville NJ. The effect of synthesis parameters on the catalytic synthesis of multiwalled carbon nanotubes using Fe-Co/$CaCO_3$ catalysts. S Afr J Chem, **62**, 67 (2009).

[21] Bahgat M, Farghali AA, El Rouby WMA, Khedr MH. Synthesis and modification of multi-walled carbon nano-tubes (MWCNTs) for water treatment applications. J Anal Appl Pyrolysis, **92**, 307 (2011). https://doi.org/10.1016/j.jaap.2011.07.002.

[22] Motchelaho MAM, Xiong H, Moyo M, Jewell LL, Coville NJ. Effect of acid treatment on the surface of multiwalled carbon nanotubes prepared from Fe–Co supported on CaCO3: correlation with Fischer–Tropsch catalyst activity. J Mol Catal A Chem, **335**, 189 (2011). https://doi.org/10.1016/j.molcata.2010.11.033.

[23] Rashidi AM, Akbarnejad MM, Khodadadi AA, Mortazavi Y, Ahmadpourd A. Single-wall carbon nanotubes synthesized using organic additives to Co-Mo catalysts supported on nanoporous MgO. Nanotechnology, **18**, 315605 (2007). https://doi.org/10.1088/0957-4484/18/31/315605.

[24] Lodya JAL, Seda T, Strydom AM, Manzini SS. Characterization of Fe/C catalysts supported on Al_2O_3, SiO_2 and TiO_2. J Phy Conf Ser, IOP Publishing, **200**, 082016 (2010).

[25] Hall BD, Zanchet D, Ugarte D. Estimating nanoparticle size from diffraction measurements. J Appl Cryst, **33**, 1335 (2000). https://doi.org/10.1107/S0021889800010888.

[26] Ratković S, Kiss E, Bošković G. Synthesis of high-purity carbon nanotubes over alumina and silica supported bimetallic catalysts. Chem Ind Chem Eng Q, **15**, 263 (2009). https://doi.org/10.2298/CICEQ0904263R.